Applied Catalysis A: General 464–465 (2013) 191–199

Contents lists available at SciVerse ScienceDirect

Applied Catalysis A: General

journal homepage: www.elsevier.com/locate/apcata

Solventless acetalization of glycerol with acetone to fuel oxygenates over Ni–Zr supported on mesoporous activated carbon catalyst

M.S. Khayoon, B.H. Hameed*

School of Chemical Engineering, Engineering Campus, Universiti Sains Malaysia, 14300 Nibong Tebal, Penang, Malaysia

ARTICLE INFO

Article history:
Received 22 December 2012
Received in revised form 19 May 2013
Accepted 24 May 2013
Available online xxx

Keywords:
Glycerol
Acetals
Acetalization
Catalyst
Fuel additives

ABSTRACT

Glycerol was selectively converted to branched oxygenated compounds (five membered ring solketal, **5**, and six membered ring acetal, **6**) through a solventless acetalization process with acetone catalyzed by mesoporous 5%Ni–1%Zr/AC catalyst. The reaction was carried out under nitrogen flow conditions using 0.20 g of catalyst at 45 °C. The conversion of glycerol was almost complete with corresponding selectivity of 26% and 74% toward **5** and **6** components, respectively. The catalytic activity was mainly attributed to the intercalated NiO and ZrO_2 species into the AC structure and to the surface characteristics as well. Zirconium species are essential co-catalysts with Ni species. The prepared catalysts were characterized for their intrinsic physicochemical and textural properties using BET surface area, XRD, XPS, TPR, FTIR, and EDX. The effect of different operational parameters such as reaction temperature, molar ratio of glycerol/acetone, catalyst weight and reaction time was investigated. The stability of the catalytic activity was examined through leaching and reusability tests.

1. Introduction

Due to the forecasted declining of petroleum crude, the world energy crisis has become the foremost crucial topic in this era [1,2]. Biomass-derived fuels (biofuels) are attractive alternatives to fossil fuels due to their environmentally benign and renewable nature [3]. As biodiesel is biodegradable, contains very low sulfur and toxicity, offers less emission of green house gases during combustion and good transport and storage properties, it has been categorized as “future fuel” [4,5]. The synthetic route of biodiesel via transesterification of vegetable oils with methanol furnishes glycerol as by-product with about 10 wt.% [6].

The vast increase in biodiesel industry has resulted in serious glut of glycerol in the market. Due to its high contamination with methanol, this glycerol cannot be utilized for food and pharmaceutical industries. Glycerol is an abundant carbon-neutral platform for the synthesis of variety of chemical intermediates, detergents, fuel additives, etc. [7]. Glycerol can be selectively transformed into diversified derivatives by various catalytic processes such as etherification process to obtain polyglycerols [8], oxidation process to obtain dihydroxy acetone, glyceraldehyde, glyceric acid, glycolic acid and hydroxyl pyruvic acid [9]. Furthermore, glycerol can also be transformed via esterification process with acetic acid to di- and triacetyl glycerol esters [6], dehydration process toward acrolein [10], transesterification with dimethyl carbonate to obtain glycerol carbonate [11], hydrogenolysis process to obtain propylene glycol [12], fermentation process to synthesize 1,3-propandiol [13] and by acetalization with ketones and/or aldehydes to obtain glycerol solketal and acetal [14,15].

The acetalization reaction of glycerol with aldehydes has been reported to produce branched oxygenated compounds; namely (2,2-dimethyl-[1,3]-dioxane-4-yl)-methanol (five-membered solketal, **5**) and 2,2-dimethyl-dioxane-5-ol (six-membered acetal, **6**), as shown in Scheme 1, that are currently used as fuel oxygenates [15,16]. Whereas, the catalytic acetalization of glycerol with ketones was reported to yield the five membered ring acetal (**5**) only. By viewing the previous reports for glycerol acetalization with acetone, one can observe that none of those studies presented complete glycerol conversion with no acetal (**6**) produced. In addition, 100% selectivity toward solketal and acetal (**5** and **6**) was not achieved even in supercritical conditions [17]. Moreover, hazardous solvent (dichloromethane) was used to facilitate the acetalization reaction [18]. On the other hand, the synthesis of six membered acetal (**6**) was reported only with the aldehydes-facilitated acetalization reaction of glycerol at higher temperatures [16]. The above observations are sequel to our exploration of an environmental, effective, inexpensive and more reliable route for this reaction.

In this work, glycerol was selectively converted to **5** and **6** components through a solventless acetalization process with acetone catalyzed by mesoporous Ni–Zr/AC catalyst. This paper reports the synthesis of glycerol solketal and acetal from acetone as the first approach in this field.

---

* Corresponding author. Tel.: +60 4599 6422; fax: +60 4594 1013.
E-mail address: chbassim@eng.usm.my (B.H. Hameed).

0926-860X/$ – see front matter © 2013 Elsevier B.V. All rights reserved.
http://dx.doi.org/10.1016/j.apcata.2013.05.035

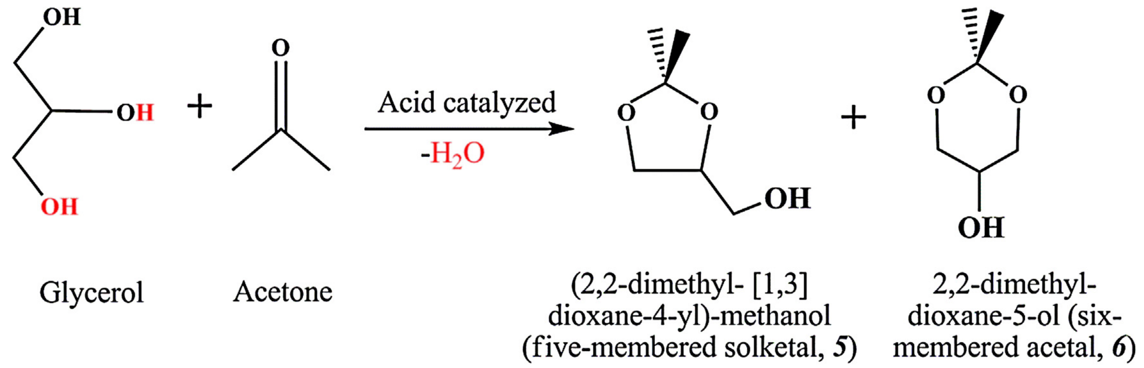

Scheme 1. Glycerol acetalization with acetone.

2. Materials and methods

2.1. Materials

Anhydrous glycerol of high purity (>99%) and sodium hydroxide (98%) were obtained from Sigma, Germany. Acetone (HPLC grade, ≥99.8%) and chromatography grade ethanol and methanol (99.7%) were supplied by Merck, Malaysia. Nickel(II) nitrate hexahydrate $Ni(NO_3)_2{\cdot}6H_2O$ and zirconium(III) chloride $ZrCl_3$ were obtained from Fluka, Germany. Activated carbon (particle size: 10–900 μm) was purchased from Galcon Carbon Corporation, USA. Hydrochloric acid (HCl 37%) from Mallinckrodt, USA was used. All reagents were used without further treatments.

2.2. Synthesis of the composite catalysts

The Ni–Zr/AC catalysts were synthesized by incipient wetness impregnation (WI) of activated carbon with an aqueous solution containing Ni(II) nitrate and/or Zr(III) chloride. Prior to metals loading, virgin AC was pretreated by 2 M HCl and 2 M NaOH solutions at 50 °C to remove the mineral matters and to eliminate their effects on the acetalization reaction. Then AC was thoroughly washed with hot distilled water until neutrality of the rinse water. For the Ni–Zr catalyst, the order of impregnation is given by the sequence of elements, i.e., Ni followed by Zr. Briefly, 5 g of AC were first impregnated with solution containing Ni (1–5 wt.%) and the resulting suspension was then left at room temperature for 24 h. Liquid was then removed by evaporation and the solid was dried in an oven at 110 °C for 6 h. Thereafter, the resultant solid was impregnated with solution of Zr(III) chloride containing the preferred amount of Zr (1–5 wt.%) and the same procedure was repeated. The as-obtained catalysts were not calcined [19], but for convenience the composition is given as the calculated amount of NiO (5%) and ZrO_2 (1%) and it was denoted as Ni–Zr/AC composite catalyst. The findings of Fidalgo et al. were interestingly noted during the catalyst preparation [20].

2.3. Catalyst characterization

The textural characteristics which include the Brunauer–Emmet–Teller (BET) surface area, pore volume and average pore diameter of the developed catalysts were characterized by nitrogen adsorption–desorption isotherms at −197 °C using Micromeritics ASAP 2020 surface area and porosity analyzer (Micromeritics Instruments Corporation, USA).

The mean metallic amounts of nickel and zirconia presented within the structure of the catalyst before and after the acetalization reaction were determined by EDX using Zeiss Supra TM 35 VP scanning electron microscope (Zeiss, Jena, Germany) coupled with FEI as a source of electrons and accelerated at 300 kV.

The identification of the surface functional groups was performed by Fourier transform infrared spectroscopy (FTIR). The IR spectra for the as-synthesized catalysts were collected on Perkin-Elmer System 2000 spectrometer using the KBr disk method. The spectra were recorded in the range of 2000–400 cm^{-1}.

Temperature-programmed reduction (TPR) was performed to determine the reduction behavior of catalysts. The experiments were performed on the Micromeritics AutoChem 2920II instrument, using 50 mg of catalyst and the temperature was increased from 35 °C to 1000 °C at a heating rate of 10 °C/min. 5%H_2 in Ar gas mixture was allowed to flow through the reactor at 15 cm^3/min. This analysis is important to elucidate the metal–support interaction in the prepared catalysts.

The verification of different surface oxidation states of Ni and Zr was based on XPS analyses. XPS spectra were acquired with a Rigaku XPS7000 spectrometer equipped with AlKα X-ray source (1486.6 eV) and a hemispherical electron analyzer. Prior to the analysis, the sample was heated to 100 °C under a flow of He gas. To investigate the influence of oxidation of the catalyst surface, the samples were, in some cases, exposed to air at 100 °C.

The structures of the synthesized materials have been investigated by wide angle XRD ($10° \leq 2\theta \leq 50°$) with a step size of 0.03° over a Bruker X-ray diffractometer (Bruker D2 Phaser Germany, 2011). The Cu K_α radiation electrons ($\lambda = 1.5406$ Å) were accelerated at 30 kV and 10 mA in an evacuated X-ray tube with Ni filter, and the data were interpreted using EVA and EXPERT software.

2.4. Catalytic reaction

All the catalytic acetalization experiments were carried out under nitrogen flow conditions and constant stirring (530 rpm). In a typical experiment, 5.0 g of anhydrous glycerol, 23.88–39.8 mL of acetone at variant molar ratios of glycerol to acetone were fed to the reaction vessel. To that, 0.20 g of the catalyst was added. The reaction media was heated to the desired reaction temperature (25–65 °C) for reaction duration of 0.5–4 h. After completion of the reaction, the catalyst was separated by centrifugation and regenerated by washing it with methanol at 45 °C and then air dried at 80 °C for 4 h to recuperate its catalytic activity.

The progress of the reaction was monitored by periodical withdrawing samples using 1 mL glass sampling syringe with 6 in. length stainless steel needle fitted to quick-fit with rubber septum. Reaction samples were quantitatively analyzed by gas chromatograph (GC; Shimadzu 2010 plus, Japan) equipped with a flame ionization detector (FID) and using a ZB5-HT capillary column (30 m × 0.25 mm × 0.25 μm). Samples for analysis were prepared by adding 10 μL of cyclohexanone as internal standard to 0.50 mL

Table 1
Textural properties of variously loaded AC catalysts.

Materials	BET surface area ($m^2\,g^{-1}$)	Total pore volume ($cm^3\,g^{-1}$)	Average pore diameter (Å)
AC	780	0.52	38.3
5% Ni/AC	582	0.46	33.6
1%Zr/AC	799	0.56	32.7
5% Ni–1%Zr/AC	612	0.38	34.2
1% Ni–5%Zr/AC	749	0.31	35.6
5% Ni–1%Zr/ACR[a]	603	0.35	32.1

[a] R stands for the spent catalyst after reusability.

of the reaction sample. About 1 μL of the final sample was then injected into the column. The column temperature was initially set at 80 °C (4 min) followed by ramping of 20 °C/min to 220 °C and then to 260 °C at 10 °C/min. The FID and injection temperatures were both fixed at 250 °C. Helium at 1.3 mL/min was used as carrier gas. The injection split ratio was 20. The reaction products were verified by qualitative analysis of reaction samples by GC/MS Perkin-Elmer system (Clarus 600 gas chromatography attached to a Clarus 600T mass spectrometer) equipped with DB-5 column.

3. Results and discussion

3.1. Catalysts characterization

3.1.1. Textural properties

The textural properties (BET surface area, pore volume and pore size) of the AC-supported catalyst samples were calculated from the N_2 adsorption–desorption isotherms at −197 °C and presented in Table 1. The surface areas of the prepared catalysts were relatively high and ranged from 582 to 799 $m^2\,g^{-1}$. According to Table 1, the surface area of the virgin AC material was found to decrease from 780 to 582 $m^2\,g^{-1}$ as 5 wt.% Ni loaded was introduced. This could be attributable to the partial occlusion of the pores due to the intercalation of metallic species and thereby leading to decrease the pore diameter and the pore volume as well. On the contrary, introducing 1 wt.% Zr to the virgin AC resulted in increasing the surface properties (surface are by 2.4% and the pore volume by 7.7%), which might be attributed to the increase in microporosity (as confirmed by the reduction in average pore diameter). The catalyst 5%Ni–1%Zr/AC has shown intermediary values of the surface properties from those obtained by 5% Ni/AC and 1%Zr/AC samples, which strongly support the above arguments. The spent 5%Ni–1%Zr/AC catalyst was also characterized to investigate the change in the textural properties after the acetalization reaction. The results unveiled a decrease in the textural parameters (surface area by 1.5%, pore volume by 7.8%, pore size by 6.2%), which is merely attributable to the change in the pores size developed as a result of the reactants' adsorption and products' desorption during the reaction. Indeed, this minute change explains the stability of the catalyst' textural properties against the stirring effect, as also confirmed in our previous work [21].

The N_2 physisorption isotherms (figure not shown) for the variously loaded AC materials with Ni and Zr species were obtained from BET analysis. All the catalyst samples exhibit the type IV nitrogen isotherm with H4 type desorption hysteresis loop, which is characteristic of mesoporous materials [22]. This could evidently explain that introducing Ni and Zr species to the AC surface did not influence the mesoporosity of the virgin surface to a great extent. It was also noticed that the size of the hysteresis loop size was reduced as the amount of Ni species loaded increased, whereas loading Zr species resulted in increasing the loop size. The big hysteresis is ascribed to the existence of pore cavities larger than the openings (throats), indicates the presence of ink-bottle shaped pores in this material [23]. The isotherm shows very slow linear increase at higher values of the relative pressure ($P/P_o > 0.2$), explaining the adsorption on the outer surface of AC material. These observations strongly correlate with the obtained results of BET surface area for the same samples.

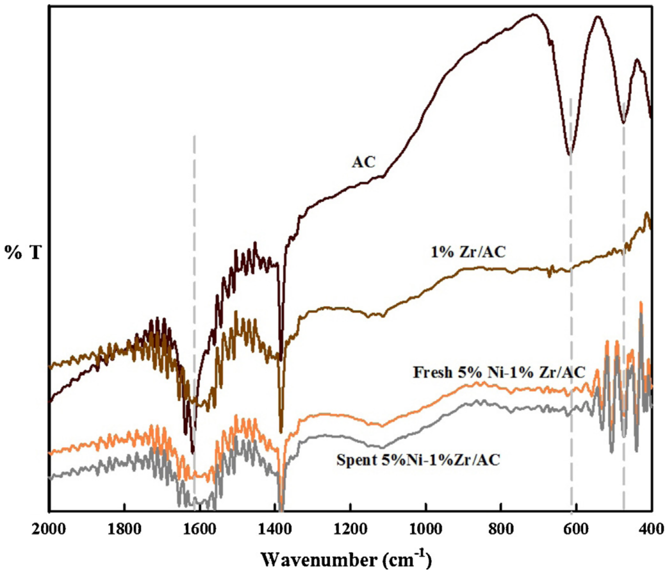

Fig. 1. (a) FTIR spectra of the virgin AC, the fresh and spent 5%Ni–1%Zr/AC and 1%Zr/AC catalysts.

In fact, three distinct regions of physisorption were presented by all the catalyst samples. The first shows a high "knee", followed by a slower growth in the adsorbed volume at low relative pressures ($P/P_o < 0.1$), which might be attributable to the intra wall monolayer adsorption. The as-shown high "knee" could simply confirm the presence of micropores on the surface of the 5% Ni–1%Zr/AC catalyst. The second region assigned at a relative pressure P/P_o 0.15 to 0.40 shows a sharp step characteristic of capillary condensation within the mesopores [19].

3.1.2. Fourier transform infrared analysis (FTIR)

Fig. 1 presents the obtained FTIR spectra of the virgin AC material and the so-developed 1%Zr/Ac and the fresh and spent 5%Ni–1%Zr/AC catalysts. The diffuse reflectance spectra for the virgin AC material showed four main bands located at 1620, 1378, 618, and 460 cm^{-1}. The IR absorptions at about 1640 cm^{-1} could be assigned to the primary amines (N—H) groups increased as observed at 1642 cm^{-1} [24], which was distorted and reduced after the loading of Ni and Zr species. This could logically explain the incorporation of metallic species to the surface of AC material, and correlate with the reduced intensity of the 1378 cm^{-1} peak after the metallic modification. The sturdy band at about 620 cm^{-1} might be ascribed to the stretching bending modes of the unsaturated C=H bonds, which was vanished after the metallic modification. Similarly, the well resolved band at about 470 cm^{-1} was also vanished, which was assigned to the C—H bonding modes. This could possibly indicate the decomposition of some of the virgin functional groups such as C—H [25] in response to the reaction with the oxides of the metallic species [26,27] and aliphatic nitro compounds C—N. Thus, the catalytic activity of 5%Ni–1%Zr/AC catalyst could be merely attributed to the presence of metallic oxides as the functional groups (NiO and ZrO_2). The interpretation of the obtained spectrum is in good agreement with the explanation reported elsewhere [19,26]. The noise presented by 5%Ni–1%Zr/AC catalyst spectrum at about 420 to 580 cm^{-1} could be ascribed to the synergistic effect of both metallic oxides.

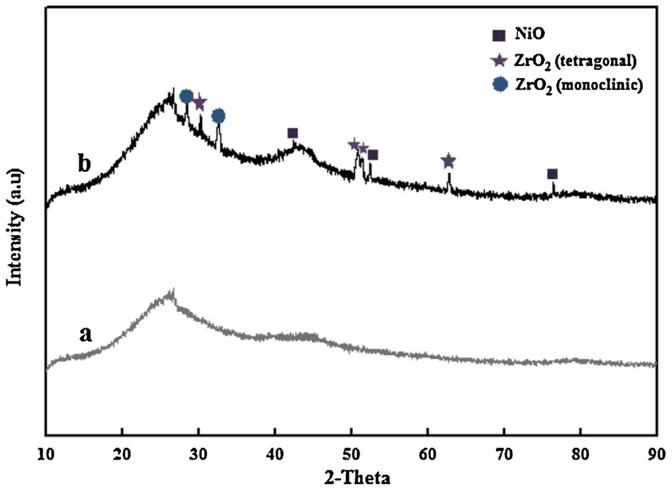

Fig. 2. XRD patterns for (a) AC; and (b) 5%Ni–1%Zr/AC catalyst. (For interpretation of the references to color in this figure legend, the reader is referred to the web version of this article.)

The obtained FTIR results suggest that NiO and ZrO_2 have substituted some of the C—H bonds in the carbon structure and should be present as intercalate and/or bounded on the pore surface. In conclusion, the structure of the as-synthesized 5%Ni–1%Zr/AC catalyst has contained the active metallic oxides species as a building component that could possibly explains the activity of this catalyst during the acetalization of glycerol with acetone. On the other hand, the spent 5%Ni–1%Zr/AC catalyst was also characterized by FTIR analysis to inspect the possible changes in its intrinsic chemical structure after the acetalization reaction. The obtained IR spectra of the spent 5%Ni–1%Zr/AC catalyst showed no appreciable change in the chemical bonding compared to the fresh catalyst sample. This can merely explains the unchanged chemical structure of this catalyst under the reaction conditions, which is logical proof of its stable chemical structure.

The confirmation of the presence of metallic oxides by FTIR alone seems insufficient and thus further characterization by XRD, TPR and XPS could help to confirm. Thus, the identification of the state of the active functional groups over 5%Ni–1%Zr/AC catalyst surface is one step ahead.

3.1.3. X-ray diffraction (XRD)

Fig. 2 shows the obtained XRD patterns of the virgin AC material and the so-modified 5%Ni–1%Zr/AC catalyst. The virgin AC material showed typical XRD pattern for the amorphous materials with distinct peak located at $2\theta = 26.2°$, which was obviously reduced after the impregnation of Ni and Zr metallic species. In the pattern of 5%Ni–1%Zr/AC catalyst, both tetragonal and monoclinic phases of ZrO_2 were observed, being the tetragonal phase was formed predominantly. The pattern shows the reflections for tetragonal zirconia at 2θ of about 30.3°, 50.8°, and at 51.4° and that for monoclinic zirconia at the 2θ of about 28.6° and 32.6°. This indicates clearly that the addition of Zr to the catalyst components resulted in the preferential formation of tetragonal ZrO_2 phase, which has the stabilization effect toward the catalyst components. It has been reported that nickel supported on the tetragonal zirconia has higher activity than that supported on the monoclinic zirconia [28]. It is therefore believed that the stabilization of NiO species by the synergistically formed tetragonal zirconia should be one of the reasons for the high activity of 5%Ni–1%Zr/AC catalyst.

Moreover, the pattern of this catalyst also shows narrow XRD peaks for metallic nickel, indicating the presence of large nickel particles within the catalyst structure. The presence of nickel oxide in the catalyst structure was toggled as the pattern unveiled the formation of monoclinic NiO phase, as obtained from EVA software. The average crystallite sizes of Ni and Zr metals have been determined by the standard Scherrer equation via analyzing the half-band widths of the peaks at $2\theta = 51.4°$ due to Ni(2 0 0) planes and $2\theta = 50.8°$ due to Zr(1 1 1) planes. The corresponding results are 18.72 and 21.38 nm for Ni and Zr, respectively. By comparing to the pore diameter of the virgin AC (38.3 Å, as obtained by BET analysis), it seems possible that both metallic particles prefer to allocate into bigger aggregates on the AC surface and interact with it through the ionic oxygen of their oxides. The herein obtained results are corroborating with those obtained by FTIR analysis and in good agreement with those reported in literature [29–31].

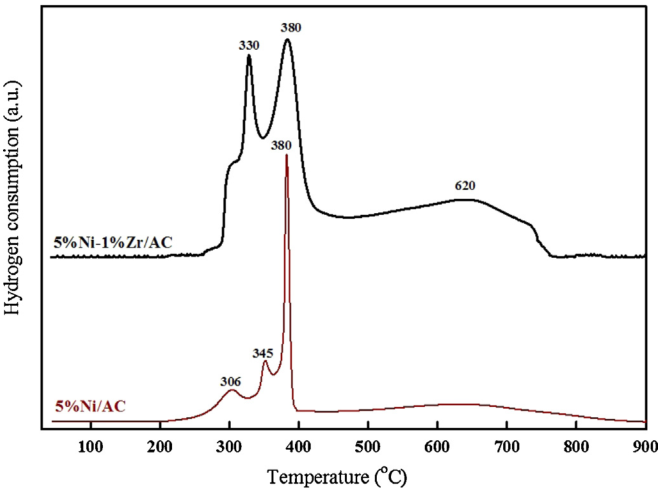

Fig. 3. TPR profiles of 5%Ni/AC and 5%Ni–1% Zr/AC catalysts.

3.1.4. H_2-TPR

Fig. 3 shows the TPR profiles for the 5%Ni/AC and 5%Ni–1%Zr/AC catalysts. It has been reported that unsupported NiO is reduced at about 280 °C [32]. However, no peaks related to the reduction of bulk NiO were found in the 5%Ni/AC and 5%Ni–1%Zr/AC catalysts. For the 5%Ni/AC catalyst, a sharp peak at 380 °C and two other low broad peaks at 306 °C and 345 °C were observed. The peak at 306 °C could be assigned to the Ni rejected from the structure, and the peak at 345 °C is associated with the reduction of NiO to Ni^0. The sharp peak at 380 °C for strongly bonded NiO species [33]. In general, the width of the peaks suggests the mode of particle size distribution, being a broad peaks correspond to broad distribution and vice versa. Thus, NiO exhibited a stronger interaction with the support in the 5%Ni–1%Zr/AC catalyst than the NiO present in 5%Ni/AC catalyst.

In the 5%Ni–1%Zr/AC catalyst, a reduction broad peak attributed to the reduction of NiO interacting with ZrO2, appeared at around 620 °C [34]. Another two peaks with lesser intensities were observed at 330 °C which is associated with NiO strongly bonded to the AC support, and at 380 °C for Ni incorporated into the Zr–AC structure [35]. From these results, it can be inferred that the addition of ZrO_2 suppressed the interaction between nickel oxide and the AC support through the formation of NiO–ZrO_2/AC composite structure.

3.1.5. X-ray photon spectroscopy (XPS)

This technique has been used to identify the chemical state of the metals on the AC surface. Therefore, the binding energies (BE) of different elements of interest like O, Ni, and Zr in the 5%Ni–1%Zr/AC catalyst were recorded. Table 2 lists the binding energies (BE) of Ni $2p_{3/2}$, Zr $3d_{3/2}$ and Zr $3d_{5/2}$ in the prepared Ni–Zr/AC catalysts. According to the literature [36], the recorded BE of metallic nickel species (Ni $2p_{3/2}$) in the 5%Ni/AC catalyst spectrum could be

Table 2
Binding energies of Ni 2p$_{3/2}$, Zr 3d$_{3/2}$ and Zr 3d$_{5/2}$ in the prepared Ni–Zr/AC catalysts.

Catalysts	Binding energies (eV)				
	Ni 2p$_{3/2}$			Zr 3d$_{3/2}$	Zr 3d$_{5/2}$
1% Zr/AC	–	–	–	185.6 (38.2%)	182.4 (61.8%)
5% Ni/AC	852.3 (13.7%)	855.7 (9.8%)	859.1 (76.5%)	–	–
1%Ni–5% Zr/AC	852.7 (10.4%)	856.2 (33.8%)	858.6 (55.8%)	184.4 (58.3%)	182.8 (41.7%)
5%Ni–1% Zr/AC	852.2 (8.9%)	856.0 (43.8%)	858.9 (47.3%)	184.4 (66.7%)	182.8 (33.3%)

interpreted as follows: 852.3, 855.7, and 859.1 eV for Ni^0, Ni^{2+}, and Ni^{2+} (satellite), respectively. Whereas, the BE in 1%Zr/AC spectrum can be assigned as follows: 185.6 and 182.4 eV for Zr 3d$_{3/2}$ and Zr 3d$_{5/2}$, respectively [37]. The recorded BE of metallic zirconium species evidently explain the presence of ZrO$_2$ in the catalyst structure (as also confirmed by XRD analysis). The X%Ni–Y%Zr/AC (X = 1 and 5, Y = 5 and 1) catalysts showed three characteristic peaks of BE of Ni 2p$_{3/2}$ and two kinds of BE of Zr 3d$_{3/2}$ and Zr 3d$_{5/2}$. When zirconium species were added to the Ni/AC structure, the BE of metallic nickel species were changed, which is possible due to the reduction Ni^0 species via oxidation modes different than the case of only nickel supported on AC.

In particular, the composition of the metallic nickel species at about 852.3 and 859.1 eV were observed to decrease in the trend of 5% Ni/AC > 1%Ni–5% Zr/AC > 5%Ni–1% Zr/AC. This trend is coincided with the increase in the composition of the zirconium metallic species (Zr 3d$_{3/2}$) and the decrease in BE of the Zr 3d$_{5/2}$. It can be said that the metallic interaction of NiO and ZrO$_2$ species is evidenced by the change of BE of each species in the X%Ni–Y%Zr/AC structure. Therefore, one can conclude that different oxidation states of NiO$_x$ species interacting with metallic ZrO$_2$ species through the formation of the synergistically bonded X%Ni–Y%Zr/AC structure. The strongly bonded metallic structure of the 1%Ni–5%Zr/AC catalyst might explain its unique catalytic performance which will be described later in this paper.

3.1.6. Elemental analysis (EDX)

The mean elemental content of the prepared catalyst was determined by EDX analysis. The results unveiled that the actual values of Ni and Zr loading were close to the theoretical ones, being the theoretical formula of 5%Ni–1%Zr/AC contained 4.36% Ni and 0.97% Zr. These results explain the accuracy of the preparation procedure and thereby confirm the presence of both metals at the preferred loading. The elemental composition of the spent 5%Ni–1%Zr/AC catalyst was also investigated and the results showed minute drop in Ni content from 4.36% to 4.17% after the fourth reuse with unchanged elemental content of Zr.

3.2. Catalytic activity: acetalization of glycerol with acetone

To assess the catalysts performance, acetalization of glycerol with acetone was performed under nitrogen atmosphere and no oxidation products were observed. According to the results of the preliminary tests using Ni/AC catalyst and shown in Table 3, the addition of Zr species to the 5% Ni/AC catalyst seems necessary due to the leaching of Ni species from the Ni/AC catalyst and to the selective behavior of Zr species toward the formation of **6** component.

Fig. 4 compares the catalytic activity (defined as glycerol conversion) of variously loaded AC catalysts with different amounts of Ni and/or Zr during glycerol acetalization with acetone performed at different temperatures (25–65 °C). For the catalysts loaded with Ni only, the conversion of glycerol was observed to increase as the amount of Ni loaded onto AC increased from 1 to 5 wt.%, which could explain the catalytic performance of Ni species in this reaction. The increase in Ni loading resulted in increasing the number of active sites over the catalyst surface, which certainly resulted in promoting the conversion of glycerol. It is therefore believed that 5 wt.% represent the best Ni loading, which catalyzed the complete conversion of glycerol to final product containing 86% and 10% of **5** and **6** products, respectively, at 45 °C and after 3 h. Unluckily, the product mixture contained 4% of undesired side products.

Table 3
Comparison of the catalytic activity of different AC-supported heterogeneous catalysts during glycerol acetalization with acetone using glycerol to acetone molar ratio of 1:8 at 45 °C after 3 h.

Catalyst	Conversion (%)	Selectivity (%)		
		5	**6**	Others
Blank test	28	75	0	25
AC	33	81	0	19
1% Ni/AC	65	91	3	6
3% Ni	83	62	26	12
5% Ni/AC	98	86	10	4
1%Zr/AC	54	77	23	0
3% Zr/AC	57	68	32	0
5%Zr/AC	67	63	37	0

On the contrary, catalyst samples loaded with Zr only showed lower values of conversion than those obtained with the former. Increasing the amount of Zr in the catalyst from 1 to 5 wt.% resulted in increasing the conversion from 54% to 67% at 45 °C, which could be explained by the increased acidity of the catalyst surface. Higher selectivity toward **6** product (37%) was obtained over 5 wt.% Zr/AC catalyst than that obtained using 5 wt.% Ni/AC catalyst (10%) with no side products formed. This could explain the selective behavior of Zr species during the acetalization of glycerol toward the formation of five and six membered ring acetals. Thus, the selective performance of Zr and the activity of Ni species have invited us to

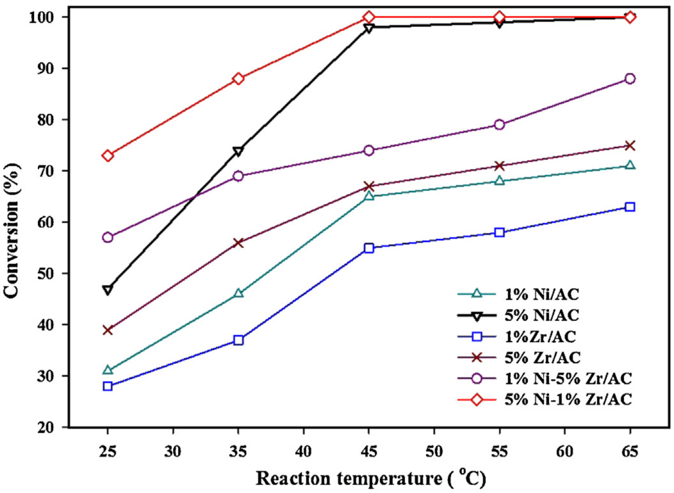

Fig. 4. Activity test performed for series of AC-supported catalysts with variant metallic loading. Reaction conditions: catalyst weight: 0.20 g; molar ratio of glycerol/acetone: 1:8; reaction temperature: 45 °C; reaction time: 3 h.

Table 4
Comparison of the catalytic activity of X%Ni–Y%Zr/AC catalysts during glycerol acetalization with acetone using glycerol to acetone molar ratio of 1:8 at 45 °C after 3 h.

Catalyst	Conversion (%)	Selectivity (%)		
		5	**6**	Others
1% Ni–1%Zr/AC	68	75	21	4
3% Ni–3%Zr/AC	73	71	29	0
5% Ni–5%Zr/AC	86	69	31	0
1% Ni–3%Zr/AC	71	74	26	0
1% Ni–5%Zr/AC	74	61	39	0
3% Ni–1%Zr/AC	81	81	17	2
3% Ni–5%Zr/AC	83	70	30	0
5% Ni–1%Zr/AC	100	74	26	0
5% Ni–3%Zr/AC	89	73	27	0

investigate a catalyst formula containing both of them in certain portions.

Therefore, catalyst formula of X%Ni–Y%Zr/AC (X and Y values vary from 1 to 5) was proposed and the corresponding samples were accordingly prepared. Catalyst samples with $X = Y = 1$, 3, and 5 have presented relatively poor catalytic activity indicated by glycerol conversion, as elucidated in Table 4. It can also be seen that the conversion of glycerol increases as the Ni loading increased. Whereas increasing Zr loading resulted in obvious increase in the selectivity toward **6** acetal product. The catalyst formula with $X = 1$ and $Y = 5$ presented higher value of selectivity toward **6** product (39%), but catalyzed the conversion of only 74% of the total glycerol fed. The catalyst formula (5%Ni–1%Zr/AC) showed the best activity among the examined catalysts, achieving complete conversion of glycerol to final product containing 74% and 26% of **5** and **6** products, respectively.

The formation of six membered ring acetal was reported only via the reaction of glycerol with aldehydes at relatively high reaction temperature. Whereas glycerol acetalization with acetone was reported to produce the **5** acetal product only [38–40]. As elucidated in Scheme 2, the formation of either five-membered ring ketal or six-membered ring acetal depends mainly on the acetalization position within glycerol molecule [40]. It is established that glycerol acetalization proceeds through a two step-mechanism, being the formation of hemiketal as the first step, followed by the removal of water molecule. The dehydration yields a tertiary carbonium ion, which can be stabilized by resonance with the non-bonded electron pairs of the adjacent oxygen atom. Afterward, a quick nucleophilic attack of the secondary hydroxyl group occurs to yield ketal (**5**) and another nucleophilic attack of the terminal hydroxyl group occurs to yield acetal (**6**). The mode of protonation of this intermediate leads to the formation of either **5** or **6** product [39]. The formation of ketal (**5**) or acetal (**6**) is strongly affected by electronic and steric factors, but it is generally accepted that the rate determining step of acetalisation is the formation of a cation from the protonated hemiketal [15]. To increase the low rate of hemiketal formation, the reaction media must be highly acidic to enhance effective protonation of any hemiketal formed, and sufficiently polar to allow stabilization of the cationic intermediate. It is therefore believed in this study that the strong acidic sites of the 5%Ni–1%Zr/AC catalyst enhanced the parallel protonation of the formed intermediate to form five and six membered ring components. Therefore, the novel results obtained in this work can be considered as the firstly achieved via glycerol reaction with acetone.

The difference in catalytic activity was attributed to the variant concentration of metallic Ni and Zr in the catalysts formulae and the catalyst acidity as well. Increasing the Ni loading in the final catalyst from 1 wt.% to 5 wt.% resulted in increasing glycerol conversion. Whereas the selectivity toward **6** acetal was found to increase as the Zr concentration in the catalyst increases. In the presence of Zr, the catalyst performance was prominently improved as indicated by the elimination of the side products. Another special phenomenon should be mentioned is that increasing Zr concentration in the catalyst resulted in minor increase in glycerol conversion, which might be attributable to the internal diffusion limitations and the non-uniform distribution of metallic aggregates into and onto the AC substrate. This conclusion is corroborating with the obtained results from XRD analysis, which stated that Zr crystallite size is larger than that of Ni.

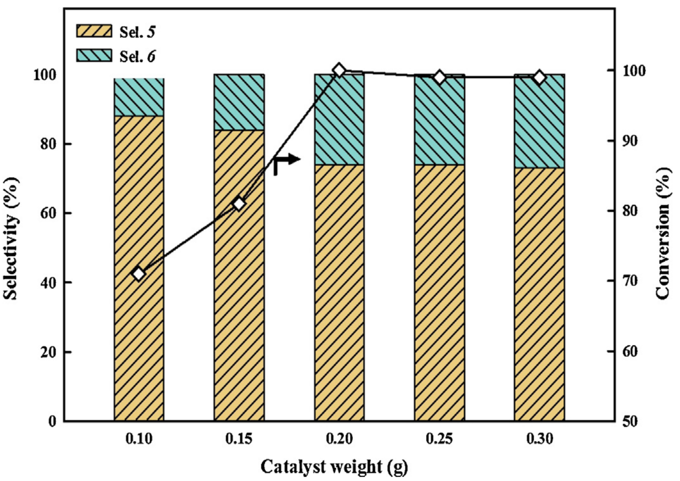

Fig. 5. Effect of catalyst weight on glycerol acetalization. Reaction conditions: molar ratio: 1:8; reaction temperature: 45 °C; reaction time: 3 h.

3.3. *Effect of reaction conditions*

3.3.1. *Effect of catalyst amount*

The reaction was performed using variant amount of 5%Ni–1%Zr/AC catalyst (0.10–0.30 g), that correspond to 2–6% of glycerol weight. The conversion of glycerol was found to increase as the amount of catalyst charged to the reactor increased, as shown in Fig. 5. This increment is expected as the number of accessible active sites over the catalyst surface increases with increasing the catalyst amount charged to the reaction vessel. As the catalyst amount increased from 0.15 to 0.20 g, glycerol conversion was significantly increased from 81% to 100% and the selectivity to 6 acetal from 16% to 26%. No appreciable changes in glycerol conversion and products selectivity were observed when the catalyst dosage increased beyond 0.20 g. The observed trend of reaction profile under variant catalyst loadings is in good agreement with other studies [15,40,41].

3.3.2. *Effect of glycerol/acetone molar ratio*

As the 0.20 g of 5%Ni–1%Zr/AC catalyst was selected as the best effective catalyst weight, further investigations were made toward the best molar ratio of reactants. Fig. 6 presents the results of glycerol conversion and products selectivity obtained using variant molar ratios of reactants. As the molar ratio increased from 1:4 to 1:8, glycerol conversion was found to linearly increase from 52% to 100% associated with decreasing the selectivity to **5** solketal and increasing that of **6** acetal. An excess of acetone employed in this reaction not only drove the forward reaction and enhanced the complete conversion of glycerol, but also promoted the formation of **6** membered ring acetal due to the increased polarity of the reaction mixture. Increasing the molar ratio to 1:10 resulted in minute decrease of glycerol conversion and the selectivity to **6** product, which might be attributed to the solubility effect of acetone to the produced acetals.

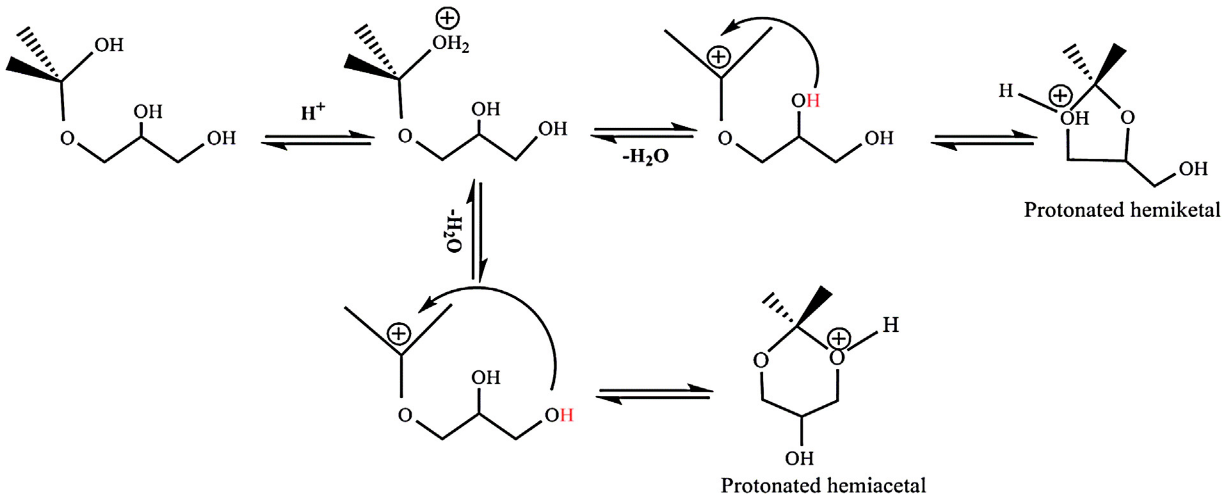

Scheme 2. Mechanism of glycerol acetalization with acetone.

When the reaction was performed at higher temperatures, the rate of acetalization was accelerated by the continuous removal of the co-produced water from the reaction media by using dean-stark apparatus [18,42,43]. The presence of water might affect the reaction pathway due to the reduced polarity of the reaction mixture. In this study, the reaction was performed at 45 °C, a temperature at which the co-produced water will be in liquid phase and the use of dean-stark system is seemingly meaningless. The results of this study seem satisfactory if compared to those reported in literature [21,40].

3.3.3. *Effect of reaction time*

The effect of reaction duration on the acetalization of glycerol was equally investigated and the obtained results are shown in Fig. 7. The conversion of glycerol was observed to increase as the reaction prolonged, which could be explained by the increased number of the reacting molecules that break the preexisting bonds and form all new bonds. From the selectivity point of view, the formation of glycerol acetals (**5** and **6** acetals) was found to be time dependent, i.e., glycerol was mainly transformed to **5** acetal product after 1 h, and the formation of **6** acetal was initiated afterward. It is worth mentioning that no proposed mechanism for the formation of **6** acetal from acetone and glycerol was found in literature. The herein observed trend of reaction profile at varied reaction times is stratifying with those reported elsewhere [16,42] and in good agreement with others [15,41].

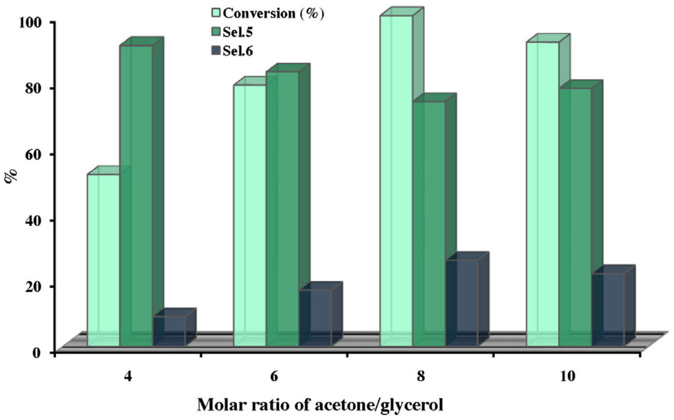

Fig. 6. Effect of acetone/glycerol molar ratio on glycerol acetalization. Reaction conditions: catalyst weight: 0.20 g; reaction temperature: 45 °C; reaction time: 3 h.

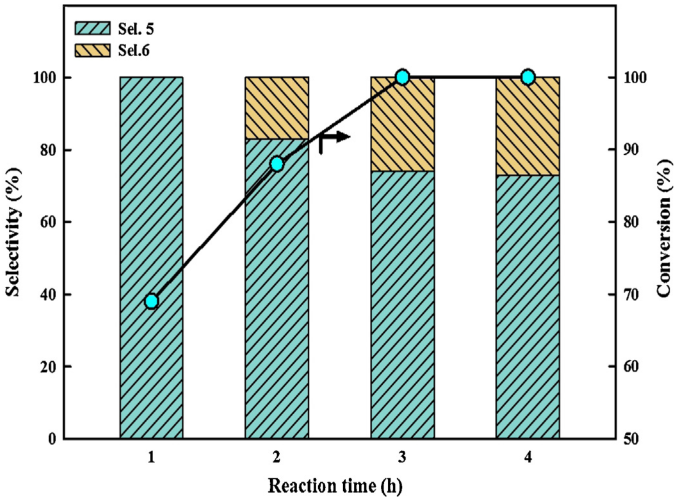

Fig. 7. Effect of reaction time on glycerol acetalization. Reaction conditions: catalyst weight: 0.20 g; acetone/glycerol molar ratio: 1:8; reaction temperature: 45 °C.

3.3.4. *Effect of reaction temperature*

The cost of glycerol acetals production can be greatly reduced by using low energy process. The impact of reaction temperature on the conversion of glycerol and products selectivity was investigated using different molar ratios of reactants and the results showed that there was a steady increase in the conversion, as presented in Table 5. Based on the outcomes as evident by glycerol conversion and the corresponding products selectivity coupled with the fact that acetalization reaction being reversible, it was found that 45 °C is the best temperature for the batch experiment. The reaction was more favored toward the formation of five membered ring acetal (**5**)

Table 5
Effect of reaction temperature on glycerol acetalization using variant molar ratios of glycerol/acetone. Reaction conditions: catalyst weight: 0.20 g; reaction time: 3 h.

Temperature (°C)	Glycerol conversion%			Sel.% (**5**)[a]	Sel.% (**6**)[a]
	1:6	1:8	1:10		
25	48	71	75	100	0
35	63	87	88	87	13
45	82	100	99	74	26
55	84	100	100	73	27
65	87	100	100	70	30

[a] The values of selectivity obtained using molar ratio of glycerol/acetone of 1:8.

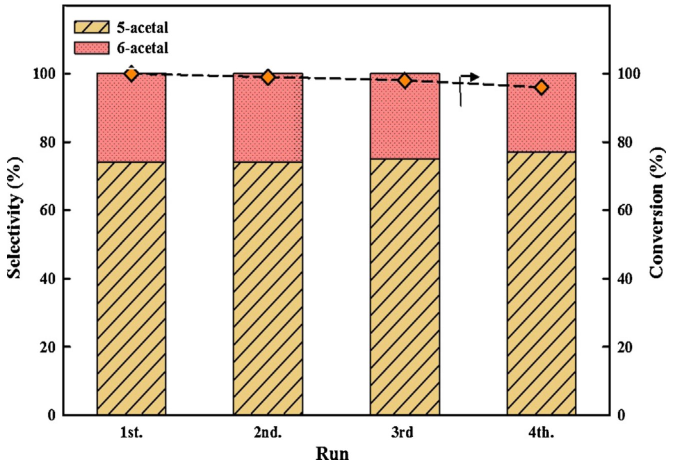

Fig. 8. Reusability test performed for 5%Ni–1%Zr/AC catalyst during glycerol acetalization. Reaction conditions: catalyst weight: 0.20 g; acetone/glycerol molar ratio: 1:8; reaction temperature: 45 °C; reaction time: 3 h.

at temperature lower than 35 °C, and its formation was obviously decreased as the temperature raised.

Based on the fact that the molecular structure of six membered ring acetal (**6**) is more complex than the five membered one (**5**), its formation was initiated after 35 °C. The observed behavior could be thermodynamically explained by the energy of formation (ΔH_f) of each product, whose value varies with the complexity of the chemical compound and strongly dependent on the reaction temperature. Therefore, the selectivity toward **6** product was observed to increase with the reaction temperature. The observed response in this study is in good agreement with the results of other studies reported in literature [39,40,43]. To this end, 45 °C was selected as the best reaction temperature at which complete glycerol conversion with corresponding selectivity of 74% and 26% toward **5** and **6** products were achieved.

3.4. Catalyst stability tests

The stability of the catalytic activity of 5%Ni–1%Zr/AC catalyst was examined via the leaching and reusability tests. The leaching test was performed according to the hot filtration method, whereas the reusability of the catalyst was tested by recycling it through four consecutive batch runs. For the leaching test, the catalyst was first immersed in 32 mL of acetone and the mixture was then heated to the reaction temperature (45 °C) and kept under constant stirring rate of 530 rpm for 3 h. Afterward, the catalyst was removed from the mixture and 5 g of glycerol were added to the hot acetone. The acetone–glycerol mixture was subjected to the same conditions described above, allowing them to react in the absence of the heterogeneous catalyst. Thereafter, the reaction sample was analyzed to determine the conversion of glycerol, which was found to be 28.7% and close to that obtained from the blank test 28.1% (blank test means the reaction of glycerol with acetone without any catalytic material). There was no appreciable leaching of the metallic components from the catalyst structure to the liquid phase, which strongly validate the claim for the stability of the prepared 5%Ni–1%Zr/AC catalyst.

After each catalytic experiment, the catalyst was separated by centrifugation, and regenerated by thoroughly washing it with methanol followed by drying it in an oven at 75 °C for 4 h. Thereafter, the regenerated catalyst was reused in another catalytic experiment. This procedure was repeated three times to achieve four consecutive recycles. Fig. 8 conspicuously presents the obtained results for glycerol conversion and products selectivity from the reusability test of 5%Ni–1%Zr/AC catalyst. The catalyst showed excellent stability of its catalyst activity as the conversion of glycerol reduced from 100% in the first run to about 97% in the fourth recycle. The selectivity toward **5** and **6** glycerol acetals maintained within three recycles, but minutely changed in the fourth recycle. The observed behavior of 5%Ni–1%Zr/AC catalyst is possibly attributable to its cohesive structure, as confirmed by FTIR and XRD analysis, and also to the reduced reaction temperature (45 °C) used in this work. These results suggest that this catalyst is the most industrially viable heterogeneous catalyst for the synthesis of oxygenated fuel additives (**5** and **6** glycerol acetals).

4. Conclusions

The acetalization of glycerol with acetone was carried out over 5%Ni–1%Zr/AC composite catalyst. Under the best reaction conditions (molar ratio of glycerol/acetone of 1:8, reaction temperature of 45 °C and reaction time of 3 h), glycerol was completely converted to final product containing 76% and 24% of five and six membered ring acetals. In this work, the synthesis of six membered ring acetal from acetone was successfully achieved as the first approach in this field. The superior performance of the 5%Ni–1%Zr/AC catalyst during the acetalization of glycerol is partly due to the increase in textural properties obtained when it was loaded with zirconium species, as earlier presented in Table 1. Moreover, the catalyst was reliably stable and the leaching was less than 2.1%. Industrially, the results attained in this work might contribute toward ameliorating the jeopardized biodiesel industry through utilization of its by-products.

Acknowledgements

The author gratefully acknowledges the financial support provided by the Universiti Sains Malaysia, under the Postgraduate Research Grant Scheme (PRGS, 1001/PJKIMIA/8044025).

References

[1] Z. Yaakob, M. Mohammad, M. Alherbawi, Z. Alam, K. Sopian, Renew. Sustain. Energy Rev. 18 (2013) 184–193.
[2] F. Manzano-Agugliaro, A. Alcayde, F.G. Montoya, A. Zapata-Sierra, C. Gil, Renew. Sustain. Energy Rev. 18 (2013) 134–143.
[3] J.R.d.O. Lima, Y.A. Ghani, R.B. da Silva, F.M.C. Batista, R.A. Bini, L.C. Varanda, J.E. de Oliveira, Appl. Catal. A: Gen. 445/446 (2012) 76–82.
[4] E.G. Giakoumis, C.D. Rakopoulos, A.M. Dimaratos, D.C. Rakopoulos, Renew. Sustain. Energy Rev. 17 (2013) 170–190.
[5] X. Zhang, L. Wu, R. Zhang, S. Deng, Y. Zhang, J. Wu, Y. Li, L. Lin, L. Li, Y. Wang, L. Wang, Renew. Sustain. Energy Rev. 18 (2013) 259–270.
[6] M.S. Khayoon, B.H. Hameed, Appl. Catal. A: Gen. 433/434 (2012) 152–161.
[7] A.B. Leoneti, V. Aragão-Leoneti, S.V.W.B. de Oliveira, Renew. Energy 45 (2012) 138–145.
[8] J.M. Clacens, Y. Pouilloux, J. Barrault, Appl. Catal. A: Gen. 227 (2002) 181–190.
[9] S. Gil, M. Marchena, L. Sánchez-Silva, A. Romero, P. Sánchez, J.L. Valverde, Chem. Eng. J. 178 (2011) 423–435.
[10] A. Alhanash, E.F. Kozhevnikova, I.V. Kozhevnikov, Appl. Catal. A: Gen. 378 (2010) 11–18.
[11] R. Bai, Y. Wang, S. Wang, F. Mei, T. Li, G. Li, Fuel Process. Technol. 106 (2013) 209–214.
[12] M. Balaraju, V. Rekha, P.S.S. Prasad, B.L.A.P. Devi, R.B.N. Prasad, N. Lingaiah, Appl. Catal. A: Gen. 354 (2009) 82–87.
[13] N. Rahmat, A.Z. Abdullah, A.R. Mohamed, Renew. Sustain. Energy Rev. 14 (2010) 987–1000.
[14] A. Sinhamahapatra, N. Sutradhar, M. Ghosh, H.C. Bajaj, A.B. Panda, Appl. Catal. A: Gen. 402 (2011) 87–93.
[15] H. Serafim, I.M. Fonseca, A.M. Ramos, J. Vital, J.E. Castanheiro, Chem. Eng. J. 178 (2011) 291–296.
[16] S.B. Umbarkar, T.V. Kotbagi, A.V. Biradar, R. Pasricha, J. Chanale, M.K. Dongare, A.-S. Mamede, C. Lancelot, E. Payen, J. Mol. Catal. A: Chem. 310 (2009) 150–158.
[17] D. Royon, S. Locatelli, E.E. Gonzo, J. Supercrit. Fluids 58 (2011) 88–92.
[18] J. Deutsch, A. Martin, H. Lieske, J. Catal. 245 (2007) 428–435.
[19] K. Díaz, V. García, J. Matos, Fuel 86 (2007) 1337–1344.
[20] B. Fidalgo, L. Zubizarreta, J.M. Bermúdez, A. Arenillas, J.A. Menéndez, Fuel Process. Technol. 91 (2010) 765–769.
[21] M.S. Khayoon, B.H. Hameed, Bioresour. Technol. 102 (2011) 9229–9235.

[22] K. Nowińska, R. Fórmaniak, W. Kaleta, A. Wącław, Appl. Catal. A: Gen. 256 (2003) 115–123.

[23] T. López, F. Rojas, R. Alexander-Katz, F. Galindo, A. Balankin, A. Buljan, J. Solid State Chem. 177 (2004) 1873–1885.

[24] A.P. Terzyk, J. Colloid. Interface Sci. 268 (2003) 301–329.

[25] F.S. Mohamed, W.A. Khater, M.R. Mostafa, Chem. Eng. J. 116 (2006) 47–52.

[26] X. Liang, H. Xiao, Y. Shen, C. Qi, Mater. Lett. 64 (2010) 953–955.

[27] X. Liang, M. Zeng, C. Qi, Carbon 48 (2010) 1844–1848.

[28] M. Yamasaki, M. Komori, E. Akiyama, H. Habazaki, A. Kawashima, K. Asami, K. Hashimoto, Mater. Sci. Eng. A 267 (1999) 220–226.

[29] S. Takenaka, E. Kato, Y. Tomikubo, K. Otsuka, J. Catal. 219 (2003) 176–185.

[30] Z. Bai, H. Chen, B. Li, W. Li, Int. J. Hydrogen Energy 32 (2007) 32–37.

[31] M.H. Youn, J.G. Seo, S. Park, D.R. Park, J.C. Jung, P. Kim, I.K. Song, Renew. Energy 34 (2009) 731–735.

[32] T. Wu, Q. Yan, H. Wan, J. Mol. Catal. A 226 (2005) 41–48.

[33] A.S. Larimi, S.M. Alvai, Fuel 102 (2012) 366–371.

[34] S. Xu, X. Wang, Fuel 84 (2005) 563–567.

[35] B. Koubaissy, A. Pietraszek, A.C. Roger, A. Kiennemann, Catal. Today 157 (2010) 436–439.

[36] R.V. Malyala, C.V. Rode, M. Arai, S.G. Hegde, R.V. Chaudhari, Appl. Catal. A: Gen. 193 (2000) 71–86.

[37] B.M. Reddy, P.M. Sreekanth, Y. Yamada, Q. Xu, T. Kobayashi, Appl. Catal. A: Gen. 228 (2002) 269–278.

[38] C.X.A. da Silva, C.J.A. Mota, Biomass Bioenergy 35 (2011) 3547–3551.

[39] P. Ferreira, I.M. Fonseca, A.M. Ramos, J. Vital, J.E. Castanheiro, Appl. Catal. B: Environ. 98 (2010) 94–99.

[40] P.S. Reddy, P. Sudarsanam, B. Mallesham, G. Raju, B.M. Reddy, J. Ind. Eng. Chem. 17 (2011) 377–381.

[41] G.S. Nair, E. Adrijanto, A. Alsalme, I.V. Kozhevnikov, D.J. Cooke, D.R. Brown, N.R. Shiju, Catal. Sci. Technol. 2 (2012) 1173–1179.

[42] F. Adam, M. Batagarawa, K. Hello, S. Al-Juaid, Chem. Pap. 66 (2012) 1048–1058.

[43] J.-C.M. Monbaliu, M. Winter, B. Chevalier, F. Schmidt, Y. Jiang, R. Hoogendoorn, M.A. Kousemaker, C.V. Stevens, Bioresour. Technol. 102 (2011) 9304–9307.